Controllable synthesis of self-assembly Co_3O_4 nanoflake microspheres for electrochemical performance

Controllable synthesis of self-assembly Co$_3$O$_4$ nanoflake microspheres for electrochemical performance

Fangyan Liu, Binbin Zhang, Hai Su, Haitao Zhang, Lei Zhang and Weiqing Yang

Key Laboratory of Advanced Technologies of Materials (Ministry of Education), School of Materials Science and Engineering, Southwest Jiaotong University, Chengdu 610031, People's Republic of China

E-mail: wqyang@swjtu.edu.cn

Abstract

Tuning the ratios of ethanol to water, self-assembling microspheres composed of Co$_3$O$_4$ nanoflakes are synthesized by the hydrothermal method. The scanning electron microscopy (SEM) images of as-grown samples obviously show that the dispersive multilayered structures gradually change into micro/nanobelts and cubic blocks structures, and then into the desired self-assembled microspheres with increasing ratios of ethanol to water. Also, all the x-ray diffraction (XRD) patterns evidently demonstrate that all obtained Co$_3$O$_4$ has cubic crystal structure. The corresponding synthesis mechanism is discussed in detail. More importantly, the unique self-assembling Co$_3$O$_4$ nanoflake microspheres have excellent electrochemical performance with large specific capacitance, good rate capability and excellent cycling performance, evidently presenting a potential capability of Co$_3$O$_4$ nanoflake microspheres to act as electrode materials for supercapacitors in sustainable power sources.

Keywords: controllable synthesis, micro/nanostructures, cobaltosic oxide, electrochemical performance

(Some figures may appear in colour only in the online journal)

1. Introduction

Cobaltosic oxide (Co$_3$O$_4$), a typical *p*-type semiconductor, has attracted growing attention because of its wide range of potential applications in the fields of sensors, catalysis, magnetism and so on [1–9]. Also, it is a very promising electrode material for supercapacitors due to its high theoretical specific capacitance (up to 3560 F g^{-1}), excellent electrochemical reactivity, good cycling life and low cost [10–13]. It has been proved that cobaltosic oxide with different morphologies and microstructures should present different properties [14]. Up to now, lots of different Co$_3$O$_4$ morphologies and sizes, such as nanowire [15], nanorods [16, 17], nanosheet [13, 18–19], nanonet [11], nanocubes [3], nanotubes [20], nanowalls [21], urchin-like [4, 22] and porous hollow polyhedra [12, 23], etc. have been synthesized successfully through various methods, that is, CBD method,

hydrothermal method, template-assisted method, solvothermal method and thermal oxidation [7, 15, 19, 24, 25]. Among these synthetic methods, the hydrothermal method is one of the most effective and widespread ways to synthesize different kinds of Co$_3$O$_4$ with special structures and morphologies. Experimentally, the unique nanostructures and corresponding formation mechanism of Co$_3$O$_4$ are usually ascribed to key experimental factors, including temperature, time, cobalt source, solvent volume, additives and so on. There have been a lot of efforts paid on the influence of experimental factors on the structure, morphology and formation mechanism of Co$_3$O$_4$ [1, 2]. However, the regulating effect of ratio of ethanol to water on the morphology and structure of Co$_3$O$_4$ has been little investigated to date. Herein, in order to effectively control the morphology and structure of Co$_3$O$_4$ and study the reaction process in the water-ethanol system, we present a controllable synthesis of self-assembling

Co_3O_4 nanoflake microspheres by the hydrothermal method and post-treatment process. Furthermore, a possible change mechanism was also proposed. Meanwhile, the electrochemical performance of the polycrystalline Co_3O_4 was also investigated.

2. Experimental

2.1. Synthesis of Co_3O_4 nanoflake microspheres

All the chemical reagents used were of analytical purity grade and used without further purification. Cobalt acetate tetrahydrate $(Co(CH_3COO)_2 \cdot 4H_2O, 99.5\%)$, urea $(CO(NH_2)_2, 99.0\%)$ and ethanol $(C_2H_5OH, 99.7\%)$ were purchased from Chengdu Kelon Chemical Reagent Factory. Ultrapure water was used throughout the experiment.

The different Co_3O_4 precursors were fabricated by the modified hydrothermal method described as follows. 0.623 g $Co(CH_3COO)_2 \cdot 4H_2O$ and 1.4 g $CO(NH_2)_2$ were dissolved in 20 ml solution, composed of 15 ml ultrapure water and 5 ml ethanol, under ultrasonic vibration. The as-formed mixed solution was moved to a 50 ml Teflon-lined autoclave and then sealed. The autoclave was maintained at 160 °C for 2 h and then cooled to room temperature. The precipitate was centrifuged at 10 000 rpm, washed with ultrapure water and ethanol several times, and then dried in an oven at 70 °C for 8 h. Finally, to prepare Co_3O_4, part of the precipitate obtained was annealed at 300 °C for 2 h at a heating rate of 2 °C min^{-1} in air. In order to investigate the regulating effect of the ratio of ethanol to water on Co_3O_4, this ratio (V_e/V_w) was altered from 0: 20 to 5: 15, 10: 10, 15: 5 and 20: 0; the total volume of these mixtures was always kept at 20 ml. The products obtained under these conditions were named sample-I, sample-II, sample-III, sample-IV and sample-V respectively.

2.2. Characterization and electrochemical tests

The crystal structure properties of the Co_3O_4 precursors and as-grown Co_3O_4 nanomaterials were investigated by the XPert Pro MPD (Holland) x-ray diffractometer with Cu K_a radiation ($\lambda = 0.154$ nm). The morphologies of the samples were examined by scanning electron microscopy (SEM, S4800). The electrochemical tests were carried out on a CHI660E electrochemical working station (Shanghai Chenhua Instrument, Inc.) using a typical three-electrode system in 6 M KOH. The Hg/HgO electrode was used as the reference electrode and Pt plate electrode as the counter electrode. The working electrode was prepared by mixing active materials, acetylene black and PTFE (polytetrafluoroethylene) at a weight ratio of 80:10:10. The mixture was subjected to ultrasonic vibration for 1 h, and the slurry was coated on a piece of nickel foam of area about 1 cm^2, and dried in air at 80 °C for 6 h. The working electrode was pressed to a thin foil under 10 MPa and dried overnight. The electrochemical performance of the products was investigated with cyclic voltammetry (CV) and galvanostatic charge–discharge tests. The galvanostatic charge–discharge tests were performed on Land
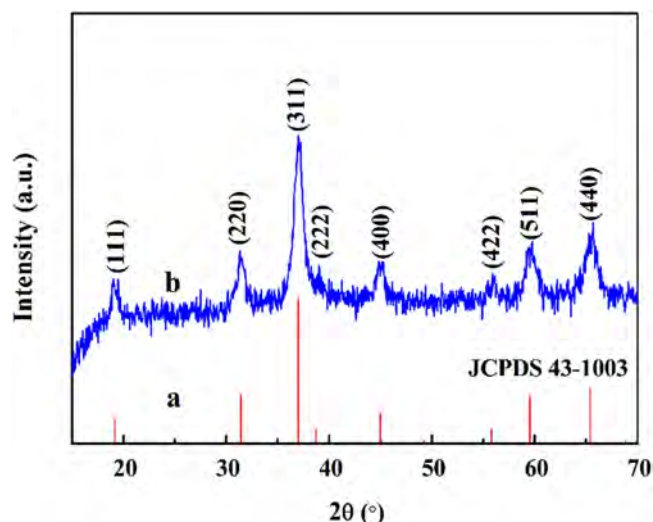
Figure 1. XRD patterns of (a) JCPDS 43-1003 and (b) sample synthesized by typical process.

Series Batteries Testing System (Wuhan Land Electronic Co., LTD).

3. Results and discussion

3.1. Morphology and structure of the Co_3O_4 nanoflake microspheres

Figure 1 shows the typical XRD pattern of as-synthesized Co_3O_4 nanoflake microspheres. All the diffraction peaks in the pattern can be well indexed to the cobalt tetroxide (Co_3O_4, JCPDS 43-1003, a = b = c = 8.084 Å) with cubic crystal structure [10, 26]. It is clearly observed that there are no characteristic peaks from other phases, evidently suggesting high purity of the as-synthesized Co_3O_4 nanoflake microspheres. Furthermore, as shown in figure 2, the SEM images of Co_3O_4 samples exhibit the spherical shape with diameters of 1–2 μm and each of them consists of nanoflakes. It is observed that the nanoflakes are radially oriented and assembled in a radial form from the center to the surface forming microspheres. The nanoflakes are interconnected with each other forming open structure with plentiful porous channels. The open channels structure would contribute to the fast penetration of the electrolyte into the porous structure and increase the contact area between electrolyte and active materials [24, 27].

3.2. Controllable synthesis of Co_3O_4 nanoflake micropheres

In order to observe the effect of ethanol concentration on the morphology of Co_3O_4 precursors, five different experiments were carried out by altering the ratio of ethanol to water, that is, 0: 20, 5: 15, 10:10, 15: 5 and 20:0; the corresponding SEM images are shown in figures 3(a)–(e) respectively. These images clearly reveal the evolution of the precursor structures over ratio of ethanol to water. At a ratio of ethanol to water of 0: 20, the multilayered structures are observed but they are
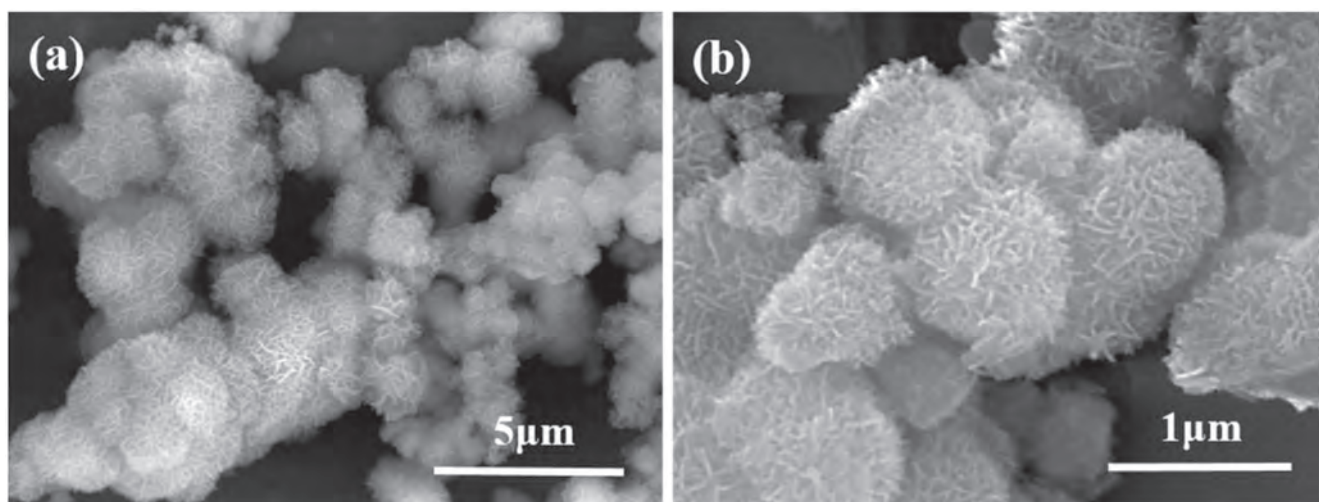
Figure 2. (a) Low and (b) high magnification SEM images of the Co_3O_4 nanoflake microspheres obtained after annealing treatment.
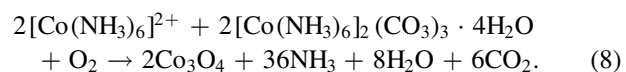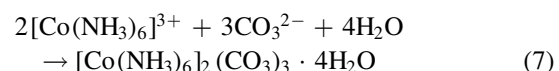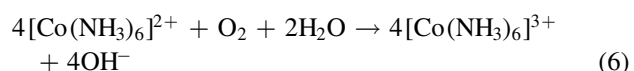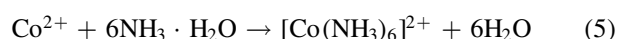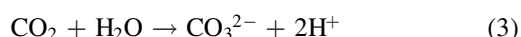
completely dispersive (figure 3(a)). When the ratio increases to 5: 15, the precursor contains two kinds of the morphologies, including mostly microbelts structures and a small number of cubic block structures (figure 3(b)). With further increase of ethanol, the microbelts are replaced stepwise by the nanobelts while the cubic block structures gradually increase. Interestingly, when the solvent is completely ethanol, all the nanobelts and cubic block structures transform into nanoflakes microspheres. Obviously, it can be concluded that the ethanol concentration has a significant regulating effect on the morphology of Co_3O_4 precursors.

3.3. Possible change mechanism

According to the ratio-dependent morphological evolution, the change process of Co_3O_4 precursors is schematically illustrated in figure 4. The morphologies of the precursors change from multilayered structures to microbelts and cubic blocks, and then to nanobelts and cubic blocks, and finally to the microspheres composed of nanoflakes. The corresponding XRD patterns of the five Co_3O_4 precursors are shown in figure 5. The main compositions of the samples I-IV are $CoCO_3$ (JCPDS 11-0692) and $[Co(NH_3)_6]_2(CO_3)_3 \cdot 4H_2O$ (JCPDS 47-0942). However, owing to increment of the amount of ethanol, the corresponding samples exhibit lower diffraction intensities and weaker crystallization properties. The diffraction intensities of sample-V are extremely weak, indicating that there are no crystals formed.

In the present synthesis system, cobalt acetate tetrahydrate dissolves in the ultrapure water to form Co^{2+}, and simultaneously urea is partly hydrolyzed to release NH_3 and CO_2 at about 70 °C, then NH_3 and CO_2 hydrolyze to produce the precipitators OH^- and CO_3^{2-}, some of the Co^{2+} combine with CO_3^{2-} to form $CoCO_3$ and the others combine with OH^- to form $Co(OH)_2$. However, the newly generated $Co(OH)_2$ is dissolved at once, while the concentration of NH_3 is relatively high in the reaction solution; instead a mass of intermediate resultant $[Co(NH_3)_6]^{2+}$ exists in the solution [28, 29], since cobalt ions tend to coordinate with six ligands

NH_3 to generate metal complexes in solutions with comparatively high concentration of NH_3 [29]. When the reaction gets going, most $[Co(NH_3)_6]^{2+}$ are immediately oxidized to $[Co(NH_3)_6]^{3+}$ by O_2 [30]. The $[Co(NH_3)_6]^{3+}$ react with the CO_3^{2-} in the solution to form the resultant $[Co(NH_3)_6]_2(CO_3)_3 \cdot 4H_2O$ crystal nuclei. The Co_3O_4 are obtained after calcination in air. The probable formation reactions of the precursors can be described in the following steps [30, 31]:

$$H_2NCONH_2 + H_2O \rightarrow 2NH_3 + CO_2 \tag{1}$$

$$NH_3 \cdot H_2O \rightarrow NH_4^+ + OH^- \tag{2}$$

$$CO_2 + H_2O \rightarrow CO_3^{2-} + 2H^+ \tag{3}$$

$$Co^{2+} + CO_3^{2-} \rightarrow CoCO_3 \tag{4}$$

$$Co^{2+} + 6NH_3 \cdot H_2O \rightarrow [Co(NH_3)_6]^{2+} + 6H_2O \tag{5}$$

$$4[Co(NH_3)_6]^{2+} + O_2 + 2H_2O \rightarrow 4[Co(NH_3)_6]^{3+} + 4OH^- \tag{6}$$

$$2[Co(NH_3)_6]^{3+} + 3CO_3^{2-} + 4H_2O \rightarrow [Co(NH_3)_6]_2(CO_3)_3 \cdot 4H_2O \tag{7}$$

$$2[Co(NH_3)_6]^{2+} + 2[Co(NH_3)_6]_2(CO_3)_3 \cdot 4H_2O + O_2 \rightarrow 2Co_3O_4 + 36NH_3 + 8H_2O + 6CO_2. \tag{8}$$

For sample-V, there is no additional free water in the solution and only a small amount of crystallization water from $Co(CH_3COO)_2 \cdot 4H_2O$ could be used. A small part of urea would hydrolyze to produce OH^- and CO_3^{2-} via equations (1)–(3) and the ethanol may release OH^- through thermal decomposition [32]. Hence, the vast majority of precipitates should be $Co(OH)_2$ even though they are not shown in the XRD pattern. This chemical process can be described by the following equations:

$$Co(CH_3COO)_2 \cdot 4H_2O \rightarrow Co^{2+} + 2CH_3COO^- + 4H_2O \tag{9}$$

$$CH_3CH_2OH + H_2O \rightarrow CH_3CH_2OH_2^+ + OH^- \tag{10}$$
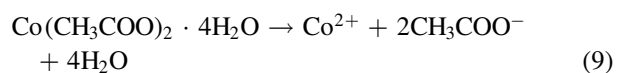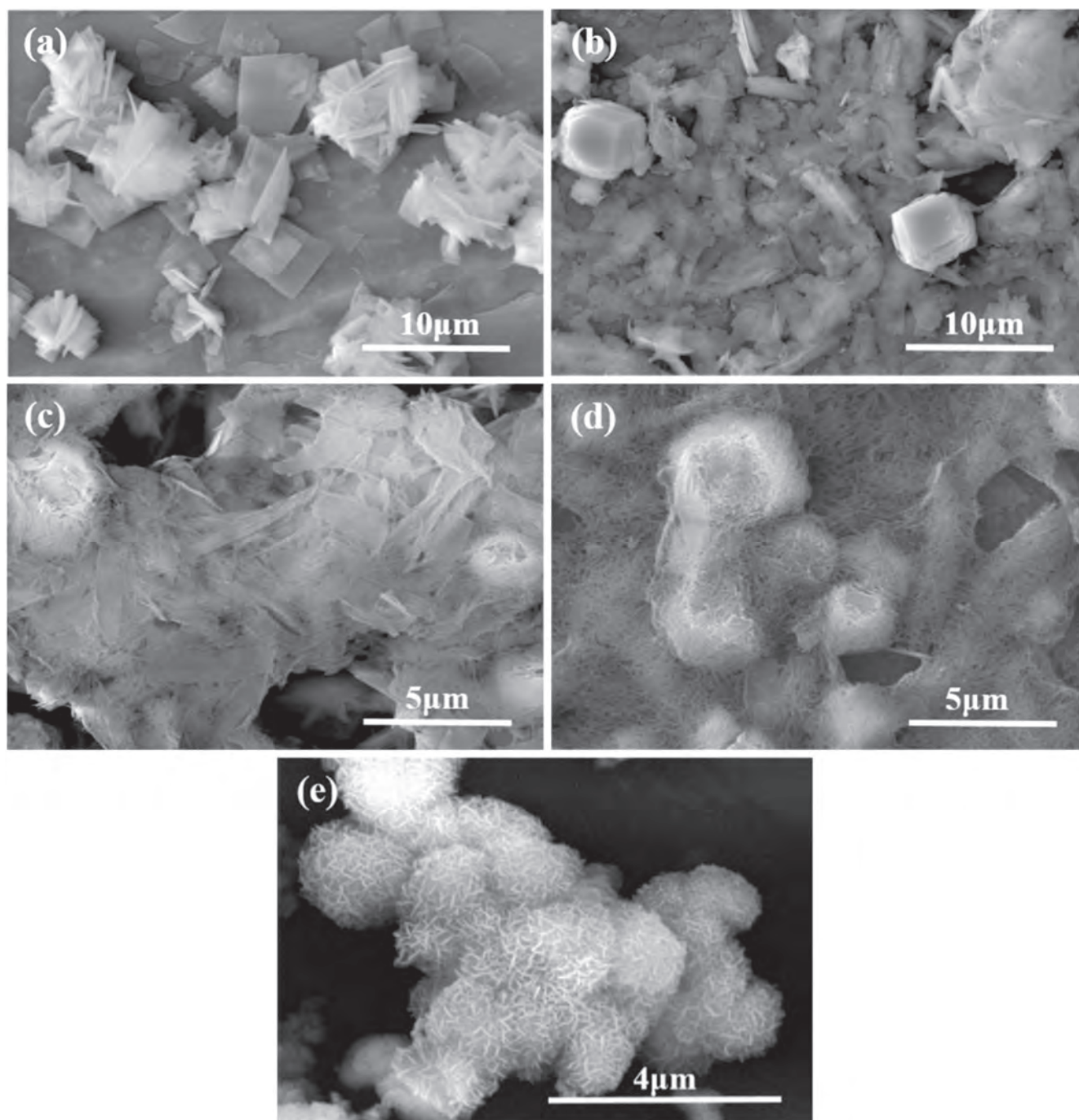
Figure 3. SEM images of tetrahydrate sample-I (a), -II (b), -III (c), -IV (d) and -V (e).

$$Co^{2+} + 2OH^- \rightarrow Co(OH)_2. \qquad (11)$$
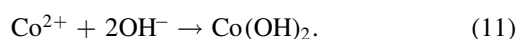
As shown in figure 3(a), the morphology of sample-I has the multilayered structures and adjacent layers bound together by weak van der Waals forces [24]. When the amount of the ethanol increases, the concentration of the as-formed crystal nuclei increases and some of the generated crystal nuclei aggregate and form cubic block structures. The higher the concentration of crystal nuclei, the more cubic blocks, which can be observed from the SEM images of the samples from I

to IV. In the meantime, as the number and size of the cubic blocks quickly increase, the reaction space in the solution becomes smaller, which limits the extended growth of the multilayered structures, then makes the multilayered structures tend to transform into microbelts and/or nanobelts with smaller size. As for sample-V, the concentration of Co^{2+} is comparatively high in the ethanol, corresponding to the better ion diffusion capability and a high supersaturation [32]. In such a highly supersaturated solution, weeny crystal nuclei are generated first, followed by crystal anisotropical growth via ion-by-ion addition [32]. The crystals tend to grow along
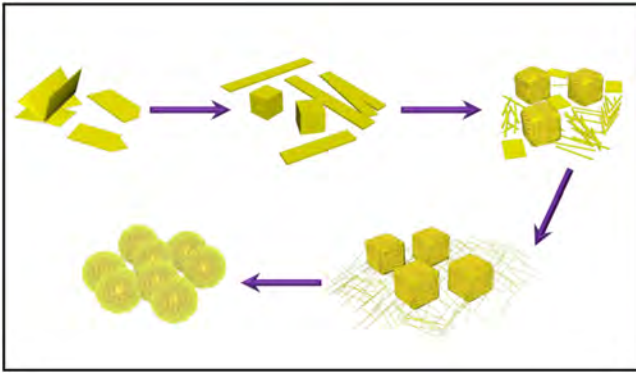
Figure 4. Schematic illustration of change mechanism of precursor structures.
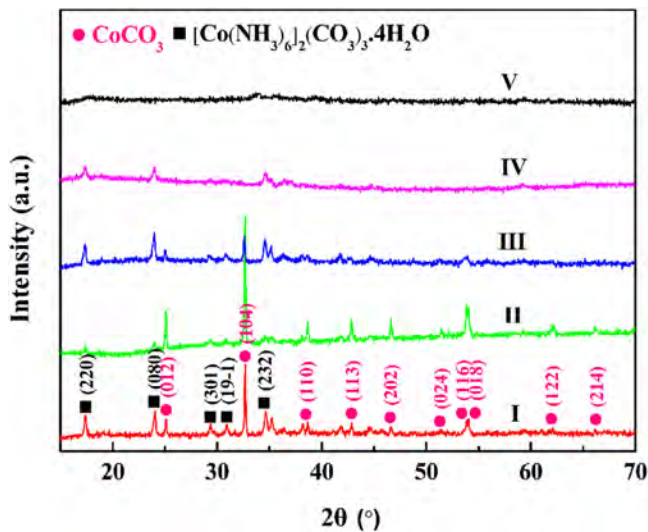
Figure 5. XRD patterns of the samples I-V obtained at different ratios of ethanol to water.
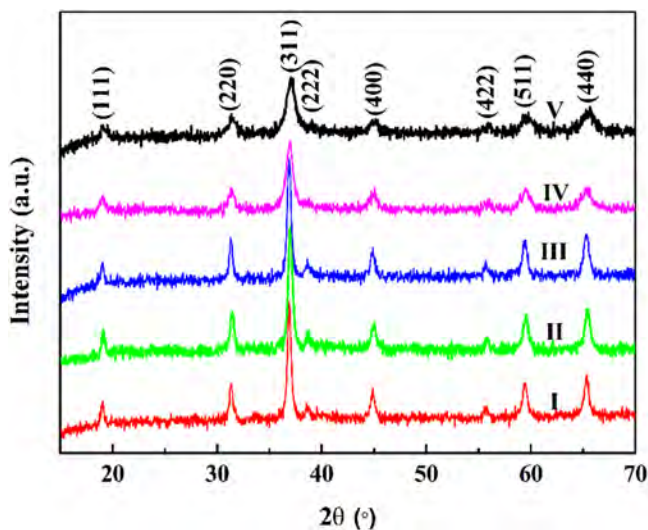

Figure 6. XRD patterns of the samples I-V annealed at 300 °C for 2 h in air.

the two-dimensional plane or three-dimensionally, hence, the $Co(OH)_2$ nanoflakes are finally acquired. These nanoflakes self-assemble with each other to form nanoflake microspheres.

In order to obtain the different Co_3O_4 structures, the precursors were finally annealed in air at 300 °C for 2 h. The XRD patterns of the annealed products are shown in figure 6. All the diffraction peaks in the XRD patterns of the five products index well to the pure cubic phase of Co_3O_4 according to the standard JCPDS (Card No.: 43-1003). This result further confirms that these precursors are decomposed completely into the Co_3O_4 phase without other phases at 300 °C. No other peaks for impurities are detected, indicating that the products are highly pure Co_3O_4. Additionally, the corresponding full width at half maximums (FWHM) of XRD peaks obviously broaden with the increasing concentration of ethanol, evidently revealing the size of as-grown nanoflake microspheres to be smaller. Furthermore, according to the Scherrer equation, the crystal size of the different Co_3O_4 samples are 22.1, 21.4, 20.2, 19.9 and 12.5 nm for sample-I, -II, -III, -IV and -V respectively. It can be seen that the crystal size of different Co_3O_4 samples decreases with the increase of ethanol ratio, which further confirms the effective influence of ethanol ratio on the morphological evolution of Co_3O_4. Therefore, the concentration of ethanol can effectively tune the crystallization properties of the Co_3O_4 nanostructures.

3.4. Electrochemical performance of Co_3O_4

The electrochemical performances of these obtained Co_3O_4 samples were studied by applying them as supercapacitor electrodes. Figure 7(a) shows the CV curves of samples I-V at the scan rate of 5 mV s^{-1} in potential range between 0 and 0.6 V. For all the samples, the CV curves exhibit obvious pseudocapacitance features, with redox peaks—which come from the redox processes of Co_3O_4/CoOOH/CoO$_2$—occurring within the electro-active materials [33–36]. The overall electrochemical processes can be expressed as follows:

$$Co_3O_4 + OH^- + H_2O \leftrightarrow 3CoOOH + e^- \qquad (12)$$

$$CoOOH + OH^- \leftrightarrow CoO_2 + H_2O + e^-. \qquad (13)$$
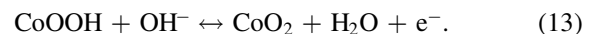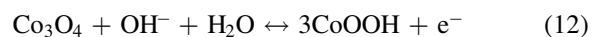
Comparing the areas under the CV curves of the samples, the area of sample-V is larger than those of other Co_3O_4 samples, which suggests that Co_3O_4 nanoflake microspheres with the ratio of ethanol to water of 20: 0 have a higher specific capacitance than other Co_3O_4 samples. In addition, the galvanostatic charge−discharge curves of samples I–V obtained in potential range 0–0.55 V at constant discharge current 0.5 A g^{-1} are shown in figure 7(b). The shapes of the GCD curves mainly show the characteristics of pseudocapacitance, which are in agreement with the result of the CV curves. The corresponding specific capacitance at a current density of 0.5 A g^{-1} of sample-I, -II, -III, -IV and -V are 160.9, 146.3, 157.3, 141.8 and 203.6 F g^{-1} respectively, which further confirms that sample-V has the best capacitive
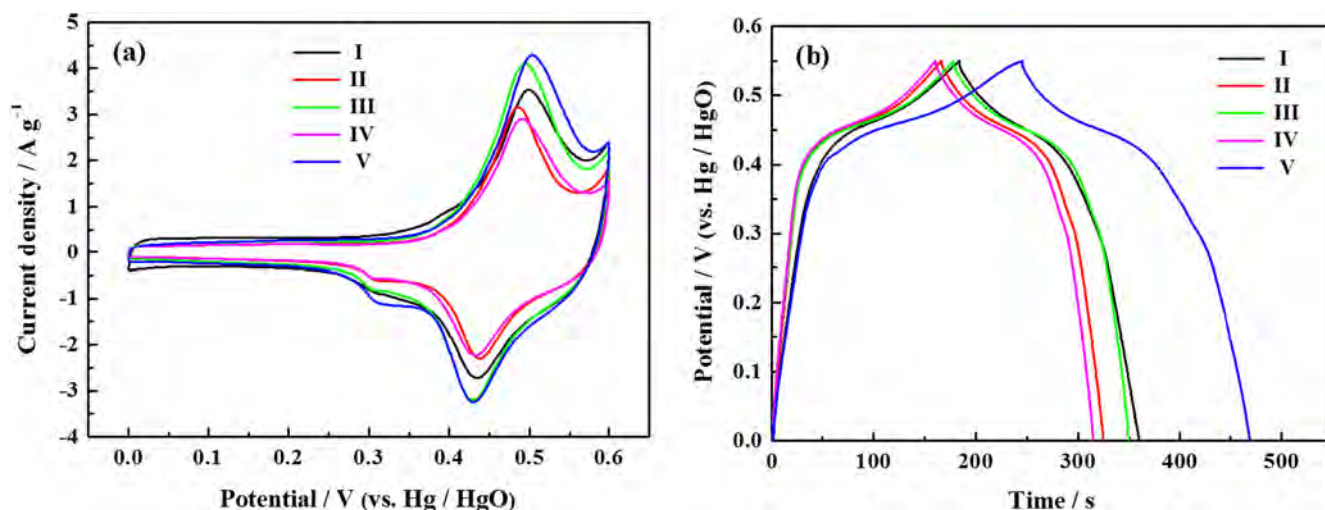
Figure 7. (a) CV curves of sample-I, -II, -III, -IV and -V at the scan rate of 5 mV s^{-1}. (b) Galvanostatic charge−discharge curves of sample-I, -II, -III, -IV and -V at a constant discharge current density of 0.5 A g^{-1}.
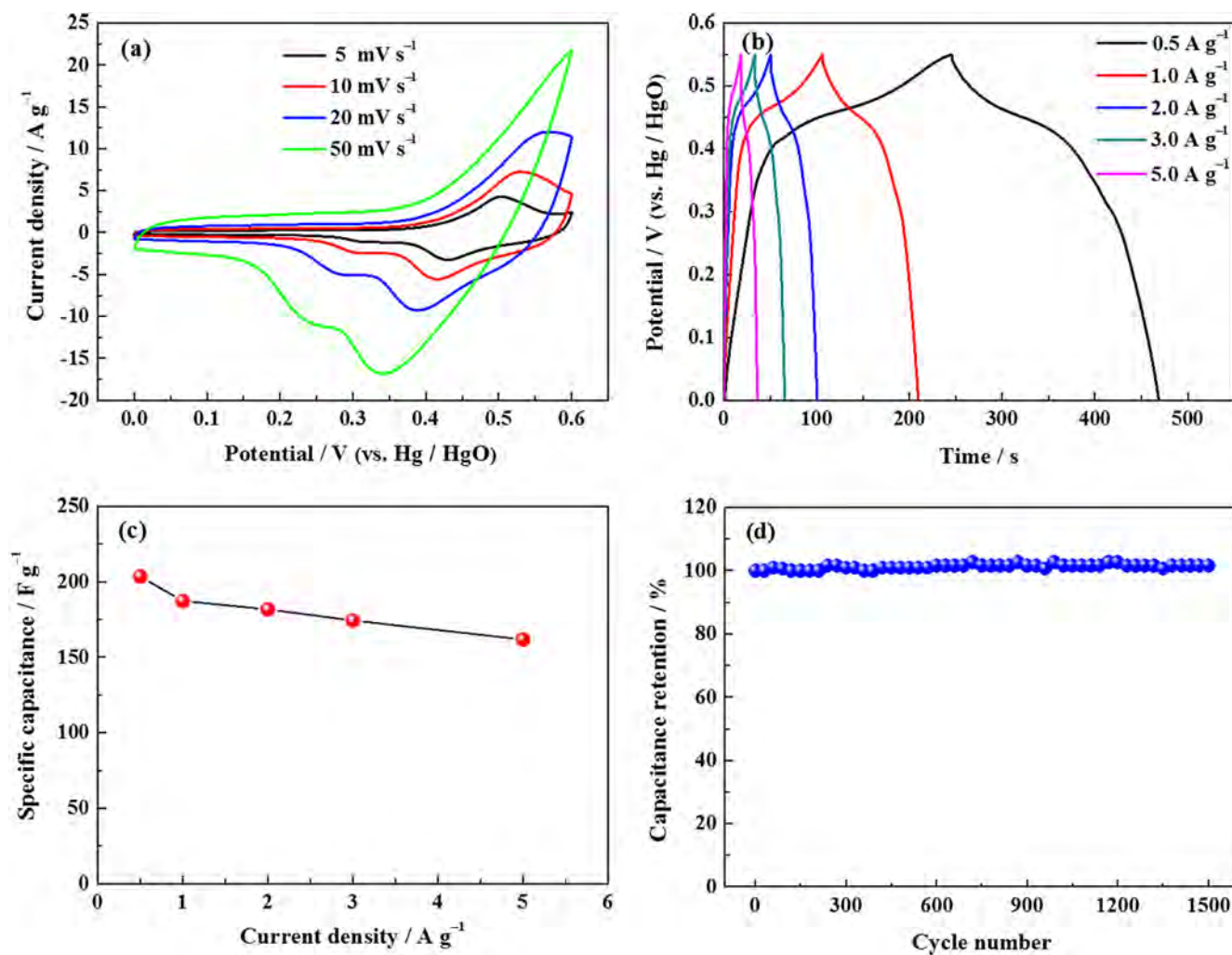
Figure 8. (a) CV curves of sample-V at different scan rates ranging from 5–50 mV s^{-1}. (b) Galvanostatic charge−discharge curves of sample-V at various current densities ranging from 0.5–5.0 A g^{-1}. (c) Specific capacitances of sample-V calculated from GCD curves at different current densities. (d) Cycling performance of sample-V after 1500 cycles at a current density of 1.0 A g^{-1}.

performance among them. The above results suggest that the open channels structure of Co_3O_4 nanoflake microspheres could provide large reaction surface area and fast transfer of ions and electrons, conducive to the improvement of electrochemical performance.

Figure 8(a) shows the CV curves of sample-V at different scan rates between 5 and 50 mV s^{-1} in the potential range from 0–0.6 V in a 6.0 mol · L^{-1} KOH aqueous electrolyte. All the curves show obvious redox peaks, which can be attributed to the conversion between different cobalt oxidation states and the corresponding faradaic reactions. With increasing scan rate, the anodic and cathodic peaks shift to higher and lower potentials respectively. The reason is that the internal part of electrode materials cannot effectively provide charge transfer quickly, and it is impossible for the electrode to transfer charge effectively with the increasing scan rate [35]. Figure 8(b) presents the galvanostatic charge−discharge curves of sample-V at various current densities in the potential window of 0–0.55 V. All the curves are symmetrical and not in a linear relationship with time, evincing pseudo-capacitive behavior. The specific capacitance of sample-V is calculated as 203.6, 187.4 181.8, 174.5 and 161.8 F g^{-1} at the current densities of 0.5, 1.0, 2.0, 3.0 and 5.0 A g^{-1} respectively. The rate capability of sample-V is shown in figure 8(c), demonstrating the relationship between the specific capacitances and current densities. It is found that the specfic capacitance decreases with the increase of the current density, and 79.4% of its initial capacitance is maintained when the current density increases from 0.5 to 5.0 A g^{-1}, demonstrating the excellent rate capability of the sample-V Co_3O_4 electrode. The decrease in specific capacitance at high current densities is caused by the charge transfer in the electrode, the ion diffusion in the electrolyte and the surface adsorption of ions on the electrode materials becoming relatively low at high current densities, which can lower the specific capacitance [37]. The cycling stability of sample-V is measured by conducting charge−discharge tests at the current density of 1.0 A g^{-1} for 1500 cycles. As shown in figure 8(d), the specific capacitance remains stable, with the capacitance retention of 101.7% after 1500 cycles, exhibiting excellent cycling stability, which is a crucial concern for an electrode material applied in supercapacitors. These results show the high specific capacitance, good rate capability and excellent cycling stability of the Co_3O_4 nanoflake microspheres, and indicate their high potential for practical supercapacitor applications.

4. Conclusion

In summary, different morphologies of Co_3O_4 were successfully synthesized via hydrothermal method and a post-anneal process in air at 300 °C for 2 h, by changing the ratio of ethanol to water. The results show that the ratio of ethanol to water has a significant controlling effect on the morphology of Co_3O_4. The as-obtained Co_3O_4 nanoflake microspheres show high electrochemical performance for supercapacitors with large specific capacitance, good rate capability and excellent cycling stability, suggesting that this is a very promising electrode material for high performance supercapacitors.

References

[1] Huang J R, Ren H B, Chen K K and Shim J J 2014 Controlled synthesis of porous Co_3O_4 micro/nanostructures and their photocatalysis property *Superlattices Microstruct.* **75** 843–56

[2] Zhou H, Lv B L, Wu D and Xu Y 2014 Synthesis of polycrystalline Co_3O_4 nanowires with excellent ammonium perchlorate catalytic decomposition property *Mater. Res. Bull.* **60** 492–7

[3] Hu L H, Peng Q and Li Y D 2008 Selective synthesis of Co_3O_4 nanocrystal with different shape and crystal plane effect on catalytic property for methane combustion *J. Am. Chem. Soc.* **130** 16136–7

[4] Zhang D E, Xie Q, Chen A M, Wang M Y, Li S Z, Zhang X B, Han G Q, Ying A L, Gong J Y and Tong Z W 2010 Fabrication and catalytic properties of novel urchin-like Co_3O_4 *Solid State Ion.* **181** 1462–5

[5] Deng S J, Chen N, Deng D Y, Li Y X, Xing X X and Wang Y D 2015 Meso- and macroporous coral-like Co_3O_4 for VOCs gas sensor *Ceram. Int.* **41** 11004–12

[6] Sahoo P, Djieutedjeu H and Poudeu P F P 2013 Co_3O_4 nanostructures: the effect of synthesis conditions on particles size, magnetism and transport properties *J. Mater. Chem.* A **1** 15022–30

[7] Vetter S, Haffer S, Wagner T and Tiemann M 2015 Nanostructured Co_3O_4 as a CO gas sensor: temperature-dependent behavior *Sens. Actuators* B **206** 133–8

[8] Liu S Y, Li L J, Ahn H S and Manthiram A 2015 Delineating the roles of Co_3O_4 and N-doped carbon nanoweb (CNW) in bifunctional Co_3O_4/CNW catalysts for oxygen reduction and oxygen evolution reactions *J. Mater. Chem.* A **3** 11615–23

[9] Liu S Y, Li L J, Patterson N A and Manthiram A 2015 Morphological transformations during *in situ* electrochemical generation of 2-dimensional Co_3O_4 hexagonal nanoplates *J. Electrochem. Soc.* **163** A150–5

[10] Deng J C, Kang L T, Bai G L, Li Y, Li P Y, Liu X G, Yang Y Z, Gao F and Liang W 2014 Solution combustion synthesis of cobalt oxides (Co_3O_4 and Co_3O_4/CoO) nanoparticles as supercapacitor electrode materials *Electrochim. Acta* **132** 127–35

[11] Wang Y, Lei Y, Li J, Gu L, Yuan H and Xiao D 2014 Synthesis of 3D-nanonet hollow structured Co_3O_4 for high capacity supercapacitor *ACS Appl. Mater. Interfaces* **6** 6739–47

[12] Zhang Y Z, Wang Y, Xie Y L, Cheng T, Lai W Y, Pang H and Huang W 2014 Porous hollow Co_3O_4 with rhombic dodecahedral structures for high-performance supercapacitors *Nanoscale* **6** 14354–9

[13] Yuan C Z, Yang L, Hou L R, Shen L F, Zhang X G and Lou X W 2012 Growth of ultrathin mesoporous Co_3O_4 nanosheet arrays on Ni foam for high-performance electrochemical capacitors *Energy Environ. Sci.* **5** 7883–7

[14] Burda C, Chen X B, Narayanan R and El-Sayed M A 2005 Chemistry and properties of nanocrystals of different shapes *Chem. Rev.* **105** 1025–102

[15] Liu W W, Li X, Zhu M H and He X 2015 High-performance all-solid state asymmetric supercapacitor based on Co₃O₄ nanowires and carbon aerogel *J. Power Sources* **282** 179–86

[16] Wang L L, Deng J A, Lou Z and Zhang T 2014 Nanoparticles-assembled Co₃O₄ nanorods p-type nanomaterials: one-pot synthesis and toluene-sensing properties *Sens. Actuators* B **201** 1–6

[17] Xing L-L, Chen Z-H and Xue X-Y 2014 Controllable synthesis Co₃O₄ nanorods and nanobelts and their excellent lithium storage performance *Solid State Sci.* **32** 88–93

[18] Meher S K and Rao G R 2011 Ultralayered Co₃O₄ for high-performance supercapacitor applications *J. Phys. Chem. C* **115** 15646–54

[19] Zhang D E, Ren L Z, Hao X Y, Pan B B, Wang M Y, Ma J J, Li F, Li S A and Tong Z W 2015 Synthesis and photocatalytic property of multilayered Co₃O₄ *Appl. Surf. Sci.* **355** 547–52

[20] Wang S M, Xiao C H, Wang P, Li Z I, Xiao B X, Zhao R, Yang T Y and Zhang M Z 2014 Co₃O₄ hollow nanotubes: facile synthesis and gas sensing properties *Mater. Lett.* **137** 289–92

[21] Xiong L Z, Teng Y, Wu Y X, Wang J J and He Z Q 2014 Large-scale synthesis of aligned Co₃O₄ nanowalls on nickel foam and their electrochemical performance for Li-ion batteries *Ceram. Int.* **40** 15561–8

[22] Hou L R, Yuan C Z, Yang L, Shen L F, Zhang F and Zhang X G 2011 Urchin-like Co₃O₄ microspherical hierarchical superstructures constructed by one-dimension nanowires toward electrochemical capacitors *RSC Adv.* **1** 1521–6

[23] Du W, Liu R M, Jiang Y W, Lu Q Y, Fan Y Z and Gao F 2013 Facile synthesis of hollow Co₃O₄ boxes for high capacity supercapacitor *J. Power Sources* **227** 101–5

[24] Pan G X, Xia X H, Cao E, Chen J and Zhang Y J 2015 Template-free synthesis of hierarchical porous Co₃O₄ microspheres and their application for electrochemical energy storage *Electrochim. Acta* **173** 385–92

[25] Zhang Y G, Liu Y, Fu S Q, Guo F and Qian Y T 2007 Morphology-controlled synthesis Of Co₃O₄ crystals by soft chemical method *Mater. Chem. Phys.* **104** 166–71

[26] Li L J, Liu S Y and Manthiram A 2015 Co₃O₄ nanocrystals coupled with O- and N-doped carbon nanoweb as a synergistic catalyst for hybrid Li-air batteries *Nano Energy* **12** 852–60

[27] Zhang H T, Zhang L, Chen J, Su H, Liu F Y and Yang W Q 2016 One-step synthesis of hierarchically porous carbons for high-performance electric double layer supercapacitors *J. Power Sources* **315** 120–6

[28] Xia X H, Tu J P, Mai Y J, Wang X L, Gu C D and Zhao X B 2011 Self-supported hydrothermal synthesized hollow Co₃O₄ nanowire arrays with high supercapacitor capacitance *J. Mater. Chem.* **21** 9319–25

[29] Feng C, Zhang J F, Deng Y D, Zhong C, Liu L and Hu W B 2015 One-pot fabrication of Co₃O₄ microspheres via hydrothermal method at low temperature for high capacity supercapacitor *Mater. Sci. Eng.* B **199** 15–21

[30] Li D W, Wu X H, Xiao T, Tao W, Yuan M, Hu X Y, Yang P and Tang Y W 2012 Hydrothermal synthesis of mesoporous Co₃O₄ nanobelts by means of a compound precursor *J. Phys. Chem. Solids* **73** 169–75

[31] Li B X, Xie Y, Wu C Z, Li Z Q and Zhang J 2006 Selective synthesis of cobalt hydroxide carbonate 3D architectures and their thermal conversion to cobalt spinel 3D superstructures *Mater. Chem. Phys.* **99** 479–86

[32] Yang W L, Gao Z, Ma J, Wang J, Wang B and Liu L H 2013 Effects of solvent on the morphology of nanostructured Co₃O₄ and its application for high-performance supercapacitors *Electrochim. Acta* **112** 378–85

[33] Duan B R and Cao Q 2012 Hierarchically porous Co₃O₄ film prepared by hydrothermal synthesis method based on colloidal crystal template for supercapacitor application *Electrochim. Acta* **64** 154–61

[34] Qing X X, Liu S Q, Huang K L, Lv K Z, Yang Y P, Lu Z G, Fang D and Liang X X 2011 Facile synthesis of Co₃O₄ nanoflowers grown on Ni foam with superior electrochemical performance *Electrochim. Acta* **56** 4985–91

[35] Park S and Kim S 2013 Effect of carbon blacks filler addition on electrochemical behaviors of Co₃O₄/graphene nanosheets as a supercapacitor electrodes *Electrochim. Acta* **89** 516–22

[36] Zhang L, Zhang H T, Jin L, Zhang B B, Liu F Y, Su H, Chun F J, Li Q H, Peng J F and Yang W Q 2016 Composition controlled nickel cobalt sulfide core–shell structures as high capacity and good rate-capability electrodes for hybrid supercapacitors *RSC Adv.* **6** 50209–16

[37] Xiang C C, Li M, Zhi M J, Manivannan A and Wu N Q 2013 A reduced graphene oxide/Co₃O₄ composite for supercapacitor electrode *J. Power Sources* **226** 65–70